Journal of Non-Crystalline Solids 34 (1979) 63–79

RAMAN SCATTERING AND NONLINEAR REFRACTIVE INDEX MEASUREMENTS OF OPTICAL GLASSES

D. HEIMAN, R.W. HELLWARTH and D.S. HAMILTON
Electronic Sciences Laboratory, University of Southern California, Los Angeles, California 90007, USA

Received 28 February 1979

The absolute Stokes–Raman scattering cross section is measured for optical glasses of varying composition, from which the nuclear contribution to the nonlinear polarizability is determined. The nonlinearities increase progressively from fluoroberyllate compositions to fluorophosphate to phosphate to silicate and finally to heavy-metal oxide glasses. Although values of the total nonlinear polarizability vary by nearly two orders-of-magnitude it is determined that the ratio of the nuclear to the electronic contribution is nearly constant and is independent of the glass composition. The electrostrictive contribution to the nonlinear polarizability is also calculated using previously measured elasto-optic constants. Correlations in the atomic structure were determined by measuring the position of the lowest-frequency Raman scattering peak and it is found that the correlation length for pure one-component glasses is larger than multicomponent glasses. Examination of the low-frequency scattering region shows that there is an excess light-scattering below 30 cm^{-1} in all glasses tested. This excess scattering in LaSF-7 was fitted between 2 to 20 cm^{-1} to a Lorentzian centered at zero frequency with a halfwidth of 2.5 ± 1 cm^{-1}, while the fit in pure silica between 5 and 30 cm^{-1} yields a halfwidth of 8 ± 3 cm^{-1}.

1. Introduction

In this paper we report the Raman spectra, calibrated absolutely, of twenty optical glasses of varying composition. In the spirit of previous work these absolute Raman-scattering cross sections are used to calculate the contribution of atomic or nuclear degrees of freedom to the nonlinear refractive index [1]. The contribution from electrostriction is also calculated from known values of the Pockels elasto-optic coefficients. Using previously determined values of the total nonlinear index [2,3], we determine a scaling law that predicts the electronic nonlinear polarizability. The glasses include: low-index beryllium–fluoride-based glasses; silicate, phosphate and fluorophosphate glasses; and high-index heavy-metal-oxide glasses. We have found in these materials that the electronic nonlinearities contribute between 60 and 85% of the self-focusing nonlinearity for optical pulses too short to be self-focused by electrostriction.

The elastic-light-scattering coefficients were also measured for these glasses in order to determine the microscopic index inhomogeneties and how they relate to the compositions. The low-frequency Raman-scattering profiles are analyzed according to the theory of Martin and Brenig [4] to estimate some correlations in the atomic structure which are then related to the network-formation properties of the particular compositions. We also analyze the low-frequency light-scattering excess (LSE) in pure silica and LaSF-7 which is centered at zero frequency. This excess was first observed in pure silica by Flubacher et al., [5] and later analyzed by Winterling [6].

2. Background

2.1. Relation of light scattering to nonlinear refraction

As is well known [1], the same physical mechanisms which give rise to light-scattering from a medium also cause a nonlinear optical response which may be described as follows. In general, when there exists a propagating electric field E in a material a polarization density P will be induced which may be expressed as a power series in the field:

$$P_i = \chi_{ij}^{(1)} E_j + \chi_{ijk}^{(2)} E_j E_k + \chi_{ijkl}^{(3)} E_j E_k E_l + \dots . \tag{1}$$

When the electric fields are of sufficient strength the nonlinear terms will give rise to measurable effects such as harmonic generation, beam self-focusing, Kerr effect and stimulated scattering processes [7,8]. In isotropic materials the lowest-order nonlinear term is cubic in the electric fields and is the one of interest for the glasses considered here. The refractive index is often expressed as $n = n_0 + n_2\langle E^2\rangle$, where n_0 and n_2 are the linear and nonlinear indices, respectively. For the case of self-focusing of laser beams there are four processes that commonly contribute: (1) electronic, (2) nuclear, (3) electrostriction, and (4) thermal. The electronic part results from induced distortions in the electronic orbitals around the nuclei and has a minimum response time of order 10^{-16} s, while the nuclear contribution arises from optical-field-induced changes in motions of the nuclei and has a response time of order 10^{-12} s. The electrostrictive contribution results from electric-field-induced strains and responds in 10^{-10}–10^{-8} s, while the thermal contribution results from absorption and will be neglected here.

When the optical frequency is below the electronic bandgap, the self-focusing index n_2 for linearly polarized light in isotropic media can be divided into electronic and nuclear contributions given by

$$n_2(\text{electronic}) = (3\pi/2n)\,\sigma_0 \tag{2}$$

and

$$n_2(\text{nuclear}) = (2\pi/n)(A_0 + B_0)\,, \tag{3}$$

where σ_0 is the electronic contribution to the third-order susceptibility and the nuclear parameters A_0 and B_0 are related to the differential scattering cross sections $d^2\sigma_i/d\Omega\, d\Delta$. The latter are defined as the fraction of incident photons of frequency ν scattered per unit distance into solid angle $d\Omega$ about ν-Δ when the incident and scattered polarizations are either parallel ($i = \parallel$) or perpendicular ($i = \perp$). From ref. [7]

$$B_0 = \frac{2c^4}{\hbar\nu} \int_0^\infty \frac{d\Delta}{\omega^3 \Delta} \frac{d^2\sigma_\perp(\nu, \Delta)}{d\Omega\, d\Delta} [1 - \exp(-\hbar\Delta/kT)] \tag{4}$$

and similarly for A_0 with $\frac{1}{2}\sigma_\parallel$-$\sigma_\perp$ substituted for $\sigma_\perp$. In practice, the total Raman scattering spectrum can be numerically integrated to give the nonlinear coefficients and hence the nonlinear index [1].

Another effect can contribute to the nonlinear properties when the optical medium is treated as an elastic continuum in which sound or long wavelength acoustic waves can exist. When a light pulse exists for a time longer than characteristic times for sound waves, ~100 ps, elasto-optic effects can contribute to the nonlinear coefficients A_0 and B_0. If the duration of the laser pulse is also longer than the time it takes for a strain to propagate across the beam diameter, then electrostriction will contribute to beam self-focusing. In order to calculate the size of this effect from eq. (4), the Brillouin cross section must be known. The integrated scattering cross sections for transverse acoustic (TA) and longitudinal acoustic (LA) phonon peaks are determined from the elasto-optic or Pockels coefficient p_{ij}. For an isotropic material, the components of the integrated scattering cross section, per phonon sideband, at right angles to the incident light is given by [9]

$$d\sigma_{VH}/d\Delta = \pi^2 n^8 kT |p_{44}|^2 / 4\lambda_0^4 \rho v_{TA}^2 \tag{5}$$

and

$$d\sigma_{VV}/d\Delta = \pi^2 n^8 kT |p_{12}|^2 / 2\lambda_0^4 \rho v_{LA}^2 , \tag{6}$$

where n is the refractive index, kT is the thermal energy, λ_0 is the wavelength of the incident light in vacuum, ρ is the mass density and v is the appropriate sound velocity. The subscripts V and H denote verticle and horizontal and refer to the polarizations of the incident and scattered light for a horizontal scattering plane. Substituting these expressions into eq. (4) and integrating, results in

$$B_0 = n^8 |p_{44}|^2 / 32\pi^2 \rho v_{TA}^2 \tag{7}$$

and

$$A_0 + B_0 = n^8 |p_{12}|^2 / 32\pi^2 \rho v_{LA}^2 , \tag{8}$$

which represent the elastic nonlinear contribution.

2.2. Model for predicting the nonlinear refractive index

Boling et al., have proposed the following empirical relation between the electronic contribution to the nonlinear refractive index $n_{2,el}$ and values of the linear refractive index and the visible optical dispersion [10]:

$$n_{2,el} = \frac{k(n_d - 1)(n_d^2 + 2)^2}{\nu[1.52 + (n_d^2 + 2)(n_d + 1)\,\nu/6n_d]^{1/2}}. \tag{9}$$

Here, the Abbé number ν is a partial dispension parameter defined as $(n_d - 1)/(n_F - n_C)$, where n_d, n_F and n_C are the indices at 587.6, 486.1 and 656.3 nm, respectively. The measured total nonlinear indices of over a dozen (solid) optical materials is fitted, to within an experimental error of (~20%) by a single value of k equal to 2.8×10^{-18} m^2 W^{-1}, ref. [3]. This is consistent with the results for the glasses we examine here, that the total nonlinear index (without electrostriction) is 75% electronic in origin.

2.3. Low-frequency light-scattering

The low-frequency light-scattering spectrum of disordered systems arising from a Debye density of states has been derived theoretically by Martin and Brenig by considering both mechanical and electrical disorder [4]. The results for polarized and depolarized components of the Stokes' spectra are [4,11]

$$I_\perp(\Delta) = A\,[n(\Delta) + 1]\,\Delta^3\,[3(v_L/v_T)^5\,e^{-(\beta\Delta/v_T)^2} + 2\,e^{-(\beta\Delta/v_L)^2}] \tag{10}$$

$$I_\parallel(\Delta) = A\,[n(\Delta) + 1]\,\Delta^3\,[2(v_L/v_T)^5\,e^{-(\beta\Delta/v_T)^2} + (15V + \tfrac{2}{3})\,e^{-(\beta\Delta/v_L)^2}] \tag{11}$$

where A is a constant, $n(\Delta) = [\exp(\hbar\Delta/kT) - 1]^{-1}$, 2β is the structural correlation length (SCL) and is the distance over which the local elasto-optic coefficients are correlated, and V is a constant that depends on depolarization. In the limit $kT >> \hbar\Delta$ the spectrum is seen to increase as Δ^2 for low frequencies and then peak at a higher frequency due to the exponential factors. Although this model was derived for the low frequency limit $\Delta < v/\beta$ we can get some idea of the value of the SCL from the peak in the depolarized spectrum as shown by Nemanich [11].

From the Raman spectrum at low frequencies it is possible to determine a characteristic distance over which the structure of the atoms is correlated. Because of wavevector non-conservation, the reduced Raman spectrum of amorphous materials follows closely the one-phonon vibrational density of states and this density of states results primarily from the short-range order in the atomic positions. The SCL is determined from the frequency of the lowest frequency peak Δ_p in the perpendicular spectrum by

$$\mathrm{SCL} \approx 2v_{TA}/\Delta_p\,. \tag{12}$$

Note that this is equivalent to finding the characteristic unit cell length, in a crystal-

line material, when the zone-boundary phonon frequency is expressed as $[(2/\pi)v_T]q_0$, where q_0 is one-half the reciprocal lattice vector, π/SCL.

3. Experimental

The experimental Raman-scattering apparatus consists of a Coherent Radiation CR3 argon ion laser, Spex 1400 3/4 meter double-grating monochromator, ITT Fw-130 photomultiplier, photon counting equipment, Hewlett Packard HP 9825 calculator and HP 6940B multiprogrammer and interface. The laser was operated at various wavelenghts between 458 and 514 nm with power output between 50 and 500 mW. The data was taken by computer program control of the spectrometer and pulse counting device. The digitized raw spectrometer traces were then modified by the computer software to give the differential scattering cross sections. The spectra were taken with right-angle scattering geometry and $f/1$ collection optics. The photomultiplier sensitivity and monochromator throughput were calibrated by a quartz–iodine standard lamp. The absolute scattering cross sections were calibrated by comparison with the polarized 992 cm^{-1} vibrational mode in benzene. For 488 nm wavelength incident light, the value used for calibration was $d\sigma/d\Omega = 2.14 \times 10^{-7}$ cm^{-1} sr^{-1} which was deduced from the results of Kato and Takuma [12].

Table 1 gives the compositions or major constituents of the glasses studied. Figs. 1 to 3 are spectrometer traces for thirteen different glasses, comprising fused quartz, two fluoroberyllates, three fluorophosphates and three phosphate glasses, and various silicate, and optically dense glasses. These spectra show the components of scattering both polarized parallel ($\parallel$) and perpendicular ($\perp$) to the incident light polarization. The spectra are calibrated against the benzene line to give the absolute Raman-scattering cross section for an excitation wavelength of 488 nm. The resolution of these traces is about 6 cm^{-1} and the uncertainties in the absolute cross sections are less than 20%. The differential cross section for pure silica has been measured previously [1], but is shown here for comparison. In all spectra, corrections are made for reflection losses at the sample surfaces, and collection angle differences due to refraction. The traces for B803 (pure BeF_2), B102, BK-3, BK-7 and SF-6 show an additional slowly varying background which is attributed to laser-induced fluorescence. The background in pure BeF_2 is well fitted to Δ^2 while all other backgrounds had to be fitted to Δ^4. These backgrounds were found to be unpolarized and were subtracted before calculating the nonlinear coefficients. For each separate glass, the exciting wavelengths were chosen so that the fluorescence in the 0–1500 cm^{-1} range was minimized. An excitation wavelength of 514 nm was chosen for SiO_2, LHG-5, LHG-6, L-248, P-224 and TaF-1; 458 nm for FK-51, B102, FK-5, BK-3, SF-6 and BK-7; and 488 nm for B803.

Fluorescence curves at visible wavelengths are shown in fig. 4, where an excitation wavelength of 458 nm was used. In some glasses, the fluorescence was as strong or stronger than the Raman signal. The fluorescence in B102, FK-51 and TaF-1 was

Table 1
Designation of glass sample materials

SiO_2:	Homosil vitreous quartz (Amersil, Inc.)
BK-3:	BSC-3 borosilicate crown (Hoya, Inc.) having the composition (wt.%): 71 SiO_2, 14 B_2O_3, 10 NaO_2, 5 Al_2O_3 ref. [18]
BK-7:	BSC-7 borosilicate crown having the composition (wt.%): 69.9 SiO_2, 9.9 B_2O_3, 8.4 NaO_2, 8.4 K_2O, 2.5 BaO ref. [18]
ED-2:	ED-4 silicate glass doped nominally with 2 wt.% Nd
ED-4:	Silicate glass undoped, having the composition (mol.%) 60 SiO_2, 27.5 Li_2O, 10 CaO, 2.5 Al_2O_3, 0.2 CeO_2
ED-8:	Silicate glass doped with Nd (similar to ED-2) having the composition (mol.%): 50 SiO_2, 28 Li_2O, 20 CaO, 2.5 Al_2O_3, 0.2 CeO, 0.8 Nd_2O_3
SF-6:	FD-6 alkali–lead–silicate glass (Hoya, Inc.) having the composition (wt.%): 27.3 SiO_2, 1.5 K_2O, 71.0 PbO ref. [18]
SF-7:	(Schott) Alkali–lead silicate glass
LaSF-7:	Dense lanthanum flint (Schott) containing mostly B_2O_3, La_2O_3 and ThO_2 with a few % Ta_2O_5 and Nb_2O_5
TaF-1:	Tantalum flint (Hoya, Inc.)
LHG-5:	Doped phosphate glass with 0.3 wt.% Nd (Hoya, Inc.)
LHG-6:	Doped phosphate glass with 0.3 wt.% Nd (Hoya, Inc.)
P-224:	Doped phosphate glass with 4.8 wt.% Nd_2O_3
L-248:	Doped fluorophosphate glass having the molar composition: 16% $Al(PO_3)_3$; 50% LiF, 33% NaF; 1% Nd_2O_3
FK-51:	Undoped fluorophosphate glass having the composition (mol.%): 23.4 SrF_2, 18.7 AlF_3, 16.2 CaF_2, 12.4 LiF, 11.9 BaF_2, 6.9 $Al(PO_3)_3$, 2.0 Al_2O_3 and 0.6 NaF
FK-5:	FC-5 fluoro crown (Hoya, Inc.)
B803:	Pure BeF_2 fluoroberyllate glass
B102:	Fluoroberyllate glass having molar composition: 48% BeF_2, 27.5% KF, 14.3% CaF_2, 10% AlF_3 (trace NdF_3)
B402:	Doped fluoroberyllate glass having molar composition: 34% BeF_2, 23% AlF_3, 19% MgF_2, 10% CaF_2, 14% BaF_2; 2.5 wt.% NdF_3

so strong that the visual color of the laser beam passing through the sample was shifted toward longer wavelengths. The fluorescent structure in B402 was so complex that it precluded accurate measurement of the Raman-scattering cross section. This material has a very steep shoulder at 475 nm in the fluorescence spectrum which was even observable when the exciting wavelength was longer. This can be understood in terms of thermal-phonon coupling to the electronic state.

In pure silica, the total (Stokes' plus anti-Stokes') polarized integrated Raman cross section was found to be $15.9 \pm 0.8 \times 10^{-8}$ cm^{-1} sr^{-1} by 488 nm incident

light. The ratio of Stokes' to Anti-Stokes' scattering is 4.0 and the ratio of the total depolarized to total polarized scattering is 0.128. The scattering cross section for the quasi-elastic peak in pure silica was found to be $4.0 \pm 8 \times 10^{-6}$ cm^{-1} sr^{-1} using 488 μm incident light. (The low-frequency scattering excess below 30 cm^{-1} is less than 1% of the total Raman cross section and was therefore not included in calculations of the nonlinear coefficients.)

Table 2 contains values of the nonlinear susceptibility parameters B_0 and $A_0 + B_0$ derived by numerically integrating the differential Raman-scattering cross sections in figs. 1 to 3 according to eq. (4). Values are also given for the quasi-elastic scattering component relative to pure silica. These values were taken in a 90° scattering geometry and are appropriate for scattering inside the sample material. This component contains all quasi-elastic scattering having a frequency shift less than ± 2 cm^{-1}, and arises primarily from the nearly elastic component of width <10 MHz. The elasto-optic or Pockels coefficients have been measured by spontaneous Brillouin scattering [9] and are used to compute the nonlinear coefficients B_0 and $A_0 + B_0$ using eqs. (7) and (8). In table 3 the various contributions to n_2 are given

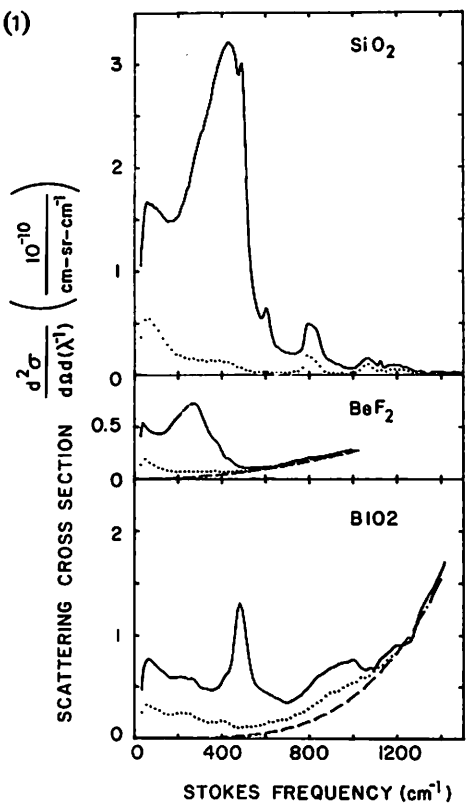

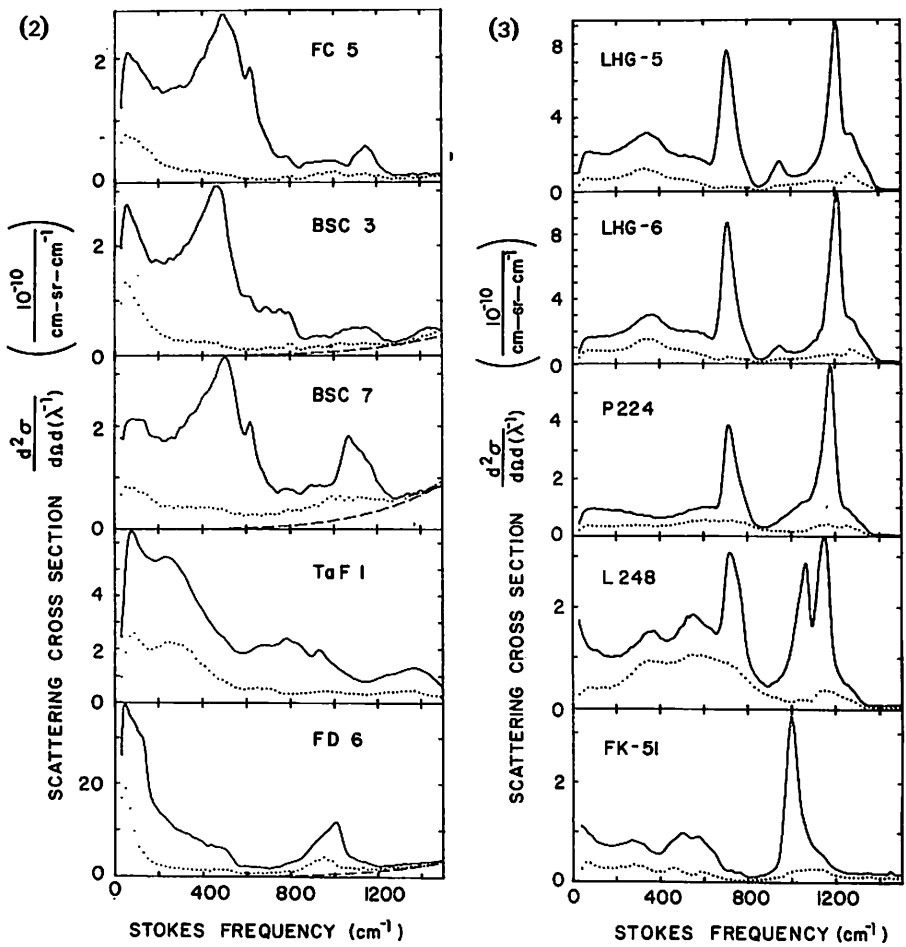

Figs. 1–3. Spectrometer traces of the absolute differential Raman-scattering cross sections per unit volume $d^2\sigma/d\Omega d(\lambda^{-1})$ plus background fluorescence, renormalized (if necessary) for 488 nm wavelength excitation, versus frequency shift for thirteen glasses. The solid curves give the polarized spectra (∥), the dotted curves give the depolarized spectra (⊥) and the dashed curves are attributed to background fluorescence. Refer to table 1 for glass compositions. The spectra of SiO_2, LHG, L248, P224 and TaF1 were taken with 514 nm wavelength excitation, FK-51, B102, FC-5, BSC-3, FD-6 and BSC-7 with 458 nm excitation and B803 (pure BeF_2) with 488 nm excitation.

for linearly polarized light. The contribution due to sound waves is calculated from eq. (3) using the appropriate nonlinear coefficients. The nuclear contribution due to the total vibrational density of states is also calculated using the nonlinear coefficients derived from the Raman cross sections. The contribution $n_2^{(el+nuc)}$ is the sum

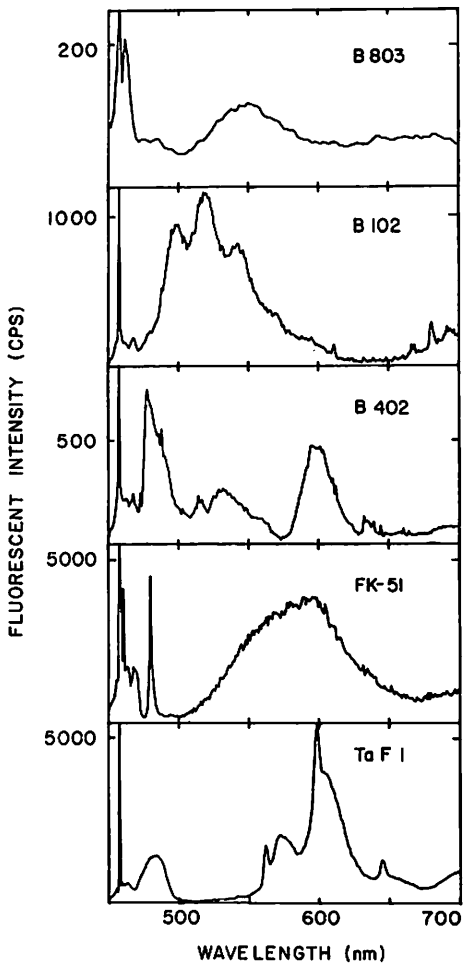

Fig. 4. Fluorescence spectra versus wavelength for B803 (pure BeF_2), B102 and B402 fluoroberyllate glasses, FK-51 fluorophosphate glass and TaF1. The excitation wavelength was 458 nm. Raman scattering from vibrations is also seen below 500 nm.

of the nuclear plus electronic parts and was either measured using time-resolved interferometry [3] or calculated from known electronic dispersion parameters according to eq. (9). Also tabulated in table 3 is the fractional part of the total n_2 that is electronic in origin.

It was noted that for frequency shifts less than 30 cm^{-1} the Raman intensity did not approach zero as expected for a Debye density-of-states as eqs. (10) and (11) show. This excess scattering was seen in all the samples and the excess intensity

Table 2

Optical and nonlinear coefficients. Linear and nonlinear optical parameters of various glasses including silicate, phosphate, fluorophosphate and fluoroberyllate types. The refractive index at 589 nm wavelength is given by n_D and at 486 nm by n_F. The quasi-elastic scattering intensity inside the material relative to that in vitreous SiO_2 has been corrected for refractive index differences. The Raman parameters were obtained by numerically integrating the absolute differential scattering cross sections of figs. 1 to 3 according to eq. (4) and the electrostrictive contributions (denoted as Brillouin) were obtained from eqs. (7) and (8) using the elasto-optical coefficients measured in ref. (9). The values for B_0 and $A_0 + B_0$ are in electrostatic units.

Glass material	Index n_D (589 nm)	Abbe number ν_d	Index n_F (486 nm)	Density (gm cm^{-3})	Quasi-elastic intensity relative to SiO_2	Raman		Brillouin	
						$10^{16} B_0$	$10^{16}(A_0 + B_0)$	$10^{16} B_0$	$10^{16}(A_0 + B_0)$
SiO_2 (Homosil)	1.462	65	1.463	2.21	≡1.0 (±20%)	15 (±20%)	58 (±15%)	14 (±30%)	69 (±15%)
BK-3	1.498	65	1.504	2.37	2.0	29	62	11	69
BK-7	1.517	64	1.522	2.51	1.6	35	67	9	56
ED-4	(1.567)	(54)	(1.573)	2.49	2.0	26	68	9	53
SF-6	1.805	25	1.828	5.19	38.	277	480	<0.5	200
SF-7	1.640	35	1.653	3.80	12.7	210	315	11	260
LaSF-7	1.921	36	1.939	5.79	60.	380	540	18	100
TaF-1	1.772	50	1.783	4.50	9.7	103	140	17	100
LHG5	1.534	63	1.543	2.67	2.4	59	110	7	90
LHG6	1.526	66	1.536	2.62	1.7	67	104	6	73
P224	1.545	(73 ± 5)	1.550	2.71	6.0	35	50	5	55
L248	1.473	(59 ± 5)	1.479	2.70	6.7	55	65	3.0	33
FK-51	1.486	(61 ± 5)	1.495	3.63	8.4	24	39	0.5	23
FK-5	1.487	70	1.492	2.45	1.8	22	54	10	80
B803(BeF_2)	1.275	107	1.277	1.99	1.2	4+2/−1	10+5/−2		
B102	1.340	100	1.342	2.60	0.40	14+4/−2	20+6/−3		
B402	1.348	98	1.386	3.25	1.8	–	–		

Table 3
Nonlinear refractive indices of glasses. Electrostrictive, nuclear, and electronic contributions to the nonlinear index of refraction of glasses. The electrostrictive contribution (es) is determined from the electro-optic coefficients of ref. [9] and the nuclear contribution (nuc) from Raman-scattering cross sections. The nuclear plus electronic contribution (el + nuc) was determined by the time-resolved interferometry measurements of ref. [3], while those denoted by the superscript a were calculated from eq. (9). The fraction of the electronic part to the electronic plus nuclear is denoted by f_e. Here n_2 is given in electrostatic units.

Glass material	Type	$10^{14}\, n_2^{(es)}$	$10^{14}\, n_2^{(nuclear)}$	$10^{14}\, n_2^{(el+nuc)}$	f^e
		(±15%)	(±15%)	(±10%)	
Silica	SiO_2	3.0	2.49	9.5	0.74
Borosilicate	BK-3	2.9	2.60	10.6 [a]	0.75
Borosilicate	BK-7	2.3	2.78	12.4	0.78
Silicate	ED-4	2.1	2.74	14.1	0.81
Dense flint	SF-6	7.0	16.7	90.0	0.81
Dense flint	SF-7	9.8	12.1	41.0 [a]	0.70
Lanthanum flint	LaSF-7	3.2	17.7	77.0 [a]	0.77
Tantalum flint	TaF-1	3.5	5.0	34.0 [a]	0.85
Phosphate	LHG5	3.7	4.5	11.6	0.61
Phosphate	LHG6	3.0	4.3	10.1	0.57
Phosphate	P224	2.2	2.03	10.3 [a]	0.80
Fluorophosphate	L248	1.4	2.76	11.3 [a]	0.76
Fluorosilicate	FK-5	3.4	2.28	10.7	0.79
Fluorophosphate	FK-51	1.0	1.64	6.9	0.76
Beryllium fluoride	BeF_2		0.49	2.3	0.79
Fluoroberyllate	B102		0.94	3.3	0.72

scaled roughly with the total Raman-scattering intensity. The polarized low-frequency Raman scattering in LaSF-7 is shown in fig. (5a), along with theoretical curve fit to eq. (11). The spectra were taken with an iodine absorption cell in order to remove the intense quasi-elastic peak and permit measurements down to less than 5 cm^{-1} shift. Data between 2 and 5 cm^{-1} were taken with a triple-passed Fabry-Perot interferometer. These spectra we also corrected for the iodine absorption away from the laser line at 514.5 nm wavelength. The "excess" intensity for LaSF-7 is shown in fig. (5b) along with a curve-fitted Lorentzian function centered at zero frequency. The halfwidth at half maximum (HWHM) was found to be $\Gamma = 2.5 \pm 1$ cm^{-1}. In pure silica the excess scattering is much more uncertain because eq. (11) can only be fit to a narrow frequency region, 35 to 50 cm^{-1}, since for low frequency the LSE is appreciable and for high frequency the theoretical model breaks down. Lorentzian fits to the LSE in pure silica indicate the width to be $\Gamma = 8 \pm 3$ cm^{-1}. It was also noted that the depolarized LSE had widths similar to the polarized LSE for both materials.

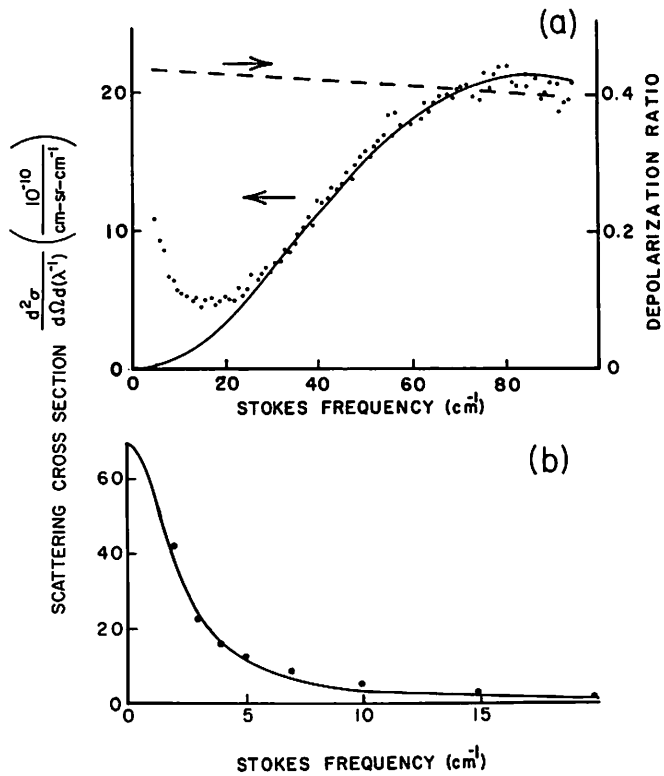

Fig. 5. In part (a) is the low-frequency absolute differential Raman-scattering cross section versus Stokes frequency shift in LaSF-7 glass for the polarized component (∥), where the broken line is the depolarization ratio, $I_\perp/I_\parallel$. The solid line is a fit to eq. (11) for data between 60 and 100 cm^{-1}. In part (b) is the excess Raman-scattering cross section [above the fit to eq. (11)]. The solid line is a Lorentzian fit having a halfwidth at half-maximum of 2.5 cm^{-1}.

4. Discussion

The Raman spectra of figs. 1 to 3 are typical of most amorphous materials. The spectra show rather broad features, and in some cases, narrow peaks at high frequencies. The spectra reflect the total vibrational density of states because the usual Raman selection rules are not obeyed in disordered materials [13]. A peak or plateau is seen in all spectra at frequencies less than 200 cm^{-1}. The scattering then drops off towards zero as Δ^2 but saturates at some small value. The cause of the light scattering excess at zero frequency is still speculative at this time, but may be related to the large sound absorption in amorphous materials [14]. The lowest frequency peak, called the "boson" peak, is due to acoustic-like excitations and reflects a Debye density-of-states. At higher frequency shifts, some of the prominent features can be associated with optic-like vibrations corresponding to internal

vibrations of common molecular units. The very broad feature at 450 cm^{-1} in silica-containing glasses is attributed to the out-of-plane rocking of the oxygen atom bridging two silicon atoms [15]. This feature probably obscures the BO_4 mode at 490 cm^{-1} in the borosilicates [16]. The large peak in BeF_2 at 270 cm^{-1} is a combination of a rocking and bending vibration of the bridging fluorine atom, while the prominent peaks in the phosphate glasses are due to the symmetric stretch of the P–O–P unit occurring at 690 cm^{-1} and 1150 cm^{-1} [17].

Since the integrated Raman cross sections are roughly proportional to the non-linear coefficients $A_0 + B_0$, we can relate the cross sections to the glass type. The fluoroberyllate glasses have the smallest cross sections, about a factor of four smaller than the low-index silicates. The fluorophosphate cross sections were slightly smaller than the low-index silicates while the phosphate cross sections were slightly larger. The materials having large refractive indices that were composed of large percentages of heavy-metal oxides have cross sections about five times that of the silicates. Now since the oxygen content increases going from fluoroberyllate to fluorophosphate to phosphate and silicate glasses, the Raman-scattering cross sections may scale roughly with oxygen content. We also note that the cross sections increase when heavy-metal oxides are added to the silicates. The quasi-elastic-peak intensity is composed almost totally of a very narrow (<10 MHz) central component which is due to scattering from refractive index inhomogeneities caused by a nearly static disorder which is quite large because it is essentially frozen-in at the glass forming temperature where the entropy fluctuations are large. The quasi-elastic scattering was found to be one to two orders-of-magnitude larger than the total Raman-shifted scattering and from table 2 it is seen that it does not scale well. The intensity is smallest for one-component glasses and is nearly equal for pure SiO_2 and pure BeF_2, while increasing when other materials are added, which is expected if the fluctuations in the homogeneity increases for multicomponent systems.

From table 3 it can be seen that the nuclear contribution relative to the electronic plus nuclear parts is nearly constant, although values vary by almost 40. The average value for f_e for the 16 glasses is 0.75 ± 0.07 and has a much smaller spread when the LHG glasses are not included. This is quite remarkable considering the wide variety of compositions and the 20% uncertainties in the measurements. Thus, we propose that the constant ratio of Raman to electronic contributions is a general rule, at least in transparent glasses. We also note that the nuclear contribution to n_2 is the same order-of-magnitude as the electrostrictive contribution, although the variations do not scale together and there does not appear to be a simple rule for choosing materials with low electrostrictive effects. When operating with long pulse laser sources, self-focusing effects may be minimized by choosing glasses containing fluorine, but here the electrostrictive contribution to n_2 may dominate.

Table 4 contains the frequencies of the boson peaks and the calculated SCL's. Also included is the thermal phonon mean free path, λ_T, calculated from $K = \frac{1}{3}C_V\bar{v}\lambda_T$, where K is the thermal conductivity, C_V is the specific heat and $\bar{v}$ is the average thermal phonon velocity. These lengths are of equal magnitude and are

Table 4

Thermal and structural lengths. Results for the average thermal mean free path λ_T and the average structural correlation length (SCL) for eighteen glass materials. In the dominant phonon approximation the thermal conductivity K is given by $K = \frac{1}{3}C_v\bar{v}\lambda_T$, where C_v is the specific heat and $\bar{v}$ is the average velocity of Debye planewaves and is taken to be the average of twice the transverse plus the longitudinal sound velocities obtained from ref. [9]. The lowest frequency peak in the VH vibrational Raman spectrum is Δ_p and the SCL is calculated from SCL = $2v_{TA}/\Delta_p$. The values in parentheses are estimated from the values of closely related materials.

Material	C_v (cal cm^{-3} °C^{-1})	K (10^{-3} cal cm^{-1} s^{-1} °C^{-1})	v_{TA} (10^5 cm s^{-1})	$\bar{v}$ (10^5 cm s^{-1})	$\Delta_p/2\pi c$ (cm^{-1})	λ_T (10^{-8} cm)	SCL (10^{-8} cm)
					±20%		
SiO_2	0.35	3.1	3.79	4.50	58	5.9	6.9
BK-3	~(0.47)	(2.7)	3.29	4.02	52	4.3	6.7
BK-7	0.51	2.66	3.65	4.45	70	3.5	5.5
ED-2		2.89	3.85	4.76	90		4.5
ED-4			3.83	4.75	90		4.5
ED-8			3.96	4.94	90		4.7
SF-6	0.48	1.40	(2.0)	(2.5)	44	3.5	4.8
SF-7	(0.42)	(1.7)	2.38	2.95	47	4.1	5.4
LaSF-7	(0.58)	(1.8)	3.56	4.22	87	2.2	4.3
TaF1			3.21	4.14	84		4.1
LHG5	0.46	2.64	3.12	3.88	70	4.4	4.7
LHG6	0.45	2.64	3.28	4.05	70	4.3	5.0
P224			3.13	3.92	70		4.7
L248			2.99	3.77	84		3.8
FK-51	0.57	2.0	3.09	3.84	68	2.7	4.8
FK-5	0.47	2.0	3.17	3.90	47	3.3	7.2
BeF_2			2.8	3.3	35		8.5
B102			(3)		56		6.0

mildly correlated. With the exception of FK-5 there is a general trend where they both increase together. This trend indicates that the thermal properties are indeed affected by the structure, which one would expect since the thermal phonons of short wavelength can be scattered by the disorder. Table 4 also shows that the one-component, SiO_2, and BeF_2, have longer SCL's than multicomponent glasses. This behavior is normal since the pure materials are known to be good network formers and there are large proportions of chain-like and network-like complexes of SiO_4 and BeF_4 tetrahedra, where nearly all of the oxygen and fluorine atoms are in bridging positions. With the addition of network modifiers such as metal oxides, large numbers of oxygen and fluorine atoms will be in non-bridging positions which will break down the network, reducing the structural correlations. We also note that the SCL to BeF_2 is larger than in SiO_2 and hence forms a better network in spite of weaker binding forces.

The low-frequency spectrum of all amorphous materials, both insulators and semiconductors is quite similar. There is a peak below 200 cm^{-1} referred to as the "boson peak" and below which the intensity decreases as Δ^2. In addition, below 20 cm^{-1} frequency shift there is a light scattering excess (LSE) that was first observed in pure silica by Flubacher et al. [5], in amorphous semiconductors [11], and in the fifteen optical glasses studied here. The temperature dependence of the LSE intensity in pure silica has been shown by Winterling to decrease faster than the one-phonon boson peak, but not as fast as a two-phonon process [6]. Winterling also proposed a mechanism for the LSE which is due to the low-frequency response of high-frequency acoustic phonons having additional relaxation as first proposed by Flude and Wagner [19]. This model can explain why the depolarization of the LSE and the boson peak are nearly equal.

The depolarization of the LSE in LaSF-7 is nearly the same as the boson peak as shown in fig. (5a). This figure also shows that there is a definite upturn in the scattering below 10 cm^{-1} which has not been seen previously in amorphous materials [11]. This glass also has a central peak in the light-scattering spectrum, first observed by Firstein et al., [20] which has the same depolarization ratio as the boson peak and a halfwidth of 0.25 cm^{-1} at room temperature as measured by Fleury and Lyons [21]. This Lorentzian peak will contribute an amount equal to $d^2\sigma/d\Omega d\Delta = 3 \times 10^{-10}$ cm^{-1} sr^{-1} cm at 2 cm^{-1} shift, which is clearly too small to contribute the observed LSE unless the central peak is non-Lorentzian. The LSE shown in fig. (5b) can be fitted reasonably well to a Lorentzian of halfwidth $\Gamma = 2.5 \pm 1$ cm^{-1} between 2 and 20 cm^{-1}. If the spectrum were only observed above 5 cm^{-1} the same fit would give a halfwidth of 6 cm^{-1}, thus we conclude that it may have a small amount of non-Lorentzian character. We also note that the frequency dependence of the sound damping of 1 cm^{-1} longitudinal acoustic phonons varies as Δ which implies a damping mechanism that has a characteristic relaxation rate of about 1 cm^{-1} [9]. Therefore, the mechanism giving rise to the LSE is a good candidate for the damping mechanism for sound waves.

A Lorentzian fit to the polarized LSE in pure silica resulted in a halfwidth of $\Gamma = 8 \pm 3$ cm^{-1}, which is more uncertain because the fit of the boson peak is more uncertain. The frequency dependence of the damping of 1 cm^{-1} longitudinal sound waves varies as Δ^2 [9]. This dependence implies that the relaxation mechanism for sound waves has a relaxation rate much greater than the phonon frequency. Again, as for LaSF-7, the mechanism giving rise to the LSE may also be responsible for the sound wave damping. The temperature dependent sound wave damping has been fit by Pine [22] and results in a relaxation rate of 16 ± 5 cm^{-1} at room temperature, which is comparable to the halfwidth of the LSE.

5. Summary

The nuclear contribution to the nonlinear optical coefficients and the nonlinear refractive indices are derived from the measured absolute differential Raman-scat-

tering cross section of sixteen different optical glasses. The magnitude of the nonlinearities is found to scale roughly with the oxygen content and is largest for oxide glasses containing heavy-metals. It was found that although the nonlinearities varied by a factor of 40, the ratio of the nuclear contribution to electronic contribution was nearly constant at $\frac{1}{3}$. This may be a general rule for glasses. A relation is also derived which relates the nonlinear coefficients for electrostriction to the Pockels elasto-optic constants, and is used to calculate the nonlinear index due to electrostriction. The structural correlation lengths are determined from the frequencies of the boson peak and the sound velocities and are found to be largest for the one-component glasses SiO_2 and BeF_2 and decrease when other materials are added. These correlation lengths are found to vary between 4 and 8 Å and are comparable to the phonon mean free paths at room temperature which are determined from the thermal conductivity. A light scattering excess for frequency shifts of less than 20 cm^{-1} was observed in fifteen different optical glasses and the scattering intensity was found to scale roughly with the intensity of the one-phonon scattering. The spectral lineshape of this excess in pure silica and LaSF-7 was determined by subtracting a theoretical fit to the boson peak and resulted in a halfwidth at half-maximum of $\Gamma = 2.5 \pm 1$ cm^{-1} for LaSF-7, and $\Gamma = 8 \pm 3$ cm^{-1} for pure silica. Finally, it is found that these widths are comparable to the relaxation rates for longitudinal sound waves, and hence the mechanism giving rise to the light scattering excess may be the same as that giving rise to the anomalously large sound wave attenuation in glasses.

Acknowledgments

We would like to thank Drs. A.J. Glass and M.J. Weber for helpful discussions and for providing excellent sample materials. The financial support of the U.S. Department of Energy through Lawrence Livermore Laboratory Subcontract No. 7509105 is greatfully acknowledged.

References

[1] R. Hellwarth, J. Cherlow and T. Yang, Phys. Rev. B11 (1975) 964.
[2] M.J. Weber, C.F. Cline, W.L. Smith, D. Milam, D. Heiman and R.W. Hellwarth, Appl. Phys. Letters 32 (1978) 403.
[3] M.J. Weber, D. Milam and W.L. Smith, Opt. Eng. 17 (1978) 463.
[4] A.J. Martin and W. Brenig, Phys. Stat. Solidi B64 (1974) 163.
[5] P. Flubacher, A.J. Leadbetter, J.A. Morrison and B.P. Stoicheff, J. Phys. Chem. Solids 12 (1959) 53.
[6] G. Winterling, Phys. Rev. B12 (1975) 2432.
[7] R.W. Hellwarth, in: Progress in Quantum Electronics (Pergamon Press, London, 1977) vol. 5.
[8] A. Yariv, Quantum Electronics, 2nd ed. (Wiley, New York, 1975).

[9] D. Heiman, D.S. Hamilton and R.W. Hellwarth, submitted to Phys. Rev. B.
[10] N.L. Boling, A.J. Glass and A. Owyoung, IEEE J. Quant. Elect. 14 (1978) 601.
[11] R.J. Nemanick, Phys. Rev. B16 (1977) 1655.
[12] Y. Kato and H. Takuma, J. Chem. Phys. 54 (1971) 5398.
[13] R. Shuker and R.W. Gammon, Phys. Rev. Letters 25 (1970) 222.
[14] N. Theodorakopoulos and J. Jäckle, Phys. Rev. B14 (1976) 2637.
[15] H. Böttger, Phys. Stat. Solidi B62 (1974) 9.
[16] R.J. Bell and D.C. Hibbins-Butler, J. Phys. C.: Solid St. Phys. 8 (1975) 787.
[17] J. Wong and C.A. Angell, Glass Structure by Spectroscopy (Marcel Dekker, New York, 1976) Ch. 7.
[18] G.W. Morey, The Properties of Glass (Reinhold, New York, 1954).
[19] P. Flude and H. Wagner, Phys. Rev. Letters 27 (1971) 1280.
[20] L.A. Firstein, J.M. Cherlow and R.W. Hellwarth, Appl. Phys. Letters 28 (1976) 25.
[21] P.A. Fleury and K.B. Lyons, Phys. Rev. Letters 36 (1976) 1188.
[22] A.S. Pine, Phys. Rev. 185 (1969) 1187.